SEMARAK ILMU PUBLISHING

Journal of Advanced Research in Applied Sciences and Engineering Technology

Journal homepage:
https://semarakilmu.com.my/journals/index.php/applied_sciences_eng_tech/index
ISSN: 2462-1943

Simulation of Trenched Coreless Silica Fiber Sensor for Refractive Index Measurement

Nazirah Mohd Razali[1], Hafizal Yahaya[1,*], Muhammad Quisar Lokman[1], Siti Nur Fatin Zuikafly[1], Fauzan Ahmad[1]

[1] Malaysia–Japan International Institute of Technology, Universiti Teknologi Malaysia, Jalan Sultan Yahya Petra, 54100 Kuala Lumpur, Malaysia

ARTICLE INFO

Article history:
Received 26 March 2023
Received in revised form 15 July 2023
Accepted 21 July 2023
Available online 30 August 2023

Keywords:
Design; simulation; no core fiber sensor; refractive index

ABSTRACT

Coreless silica fiber has garnered a lot of attention in the field of sensors. Nevertheless, the limitation of conventional and unique coreless silica fiber sensors such as complex simulation, and high fragility of its physical structure needs to be considered. This work presents a simulation of a new coreless silica fiber design in a form of a trenched coreless silica fiber sensor to overcome these limitations. To optimize the sensor's design, the trench depth was changed in the range of 0 µm to 50 µm at a fixed trench width of 50 µm. The change in analyte refractive index ranging from 1.3000 RIU to 1.4000 RIU was performed to evaluate the simulated sensing performance which showed that the increase in trench depth improved the sensor's sensitivity with 50 µm being the trench depth at which the highest sensitivity was recorded. Later, the results obtained was compared to the closest in term of design which is the standard coreless fiber. Overall, the trenched coreless silica fiber design provided better sensitivity and is highly capable as of has a new refractive index sensor with an estimated sensitivity of up to 6.62726x10-7, higher than the simulated standard coreless fiber sensor with that of 2.22053x10-7.

1. Introduction

A coreless silica fiber (CSF) or sometimes known as a no-core fiber, is a pure homogenous silica fiber [1]. In other words, CSF is an optical fiber without a core and only a solid silica rod. However, when the CSF acts as a sensor, the fiber itself becomes the core whose cladding is the air medium surrounding it. Originally, CSF was introduced to overcome the limitations of the multimode fiber (MMF), a conventional type of optical fiber sensor [2,3]. Instead of modifying the cladding layer of the MMF, CSF can be used directly as a sensor.

Since 2020, a few researchers have started introducing CSF with unique modifications such as V-shaped, S-shaped, wave-shaped, short-tapered shaped, and half-coated PDMS on D-shaped fiber, thus offering a state of art on CSF design [4-8]. These new designs are robust and have successfully overcome the fragility of the conventional CSF design such as adiabatic tapered-shaped and wet

* *Corresponding author.*
E-mail address: hafizal.kl@utm.my

https://doi.org/10.37934/araset.32.1.8794

chemical etched-shaped fiber [9-12]. Moreover, unlike the coated CSF, the unique modification does not require a sophisticated fabrication process [13-15]. Despite the good mechanical strength, the unique design suffers a complex analysis, difficult to simulate and there is no optimization carried out to study the influence of the design on the sensor sensitivity.

In this paper, we introduced a new unique simulated CSF design, namely a trenched coreless silica fiber (TCSF) via wave optic module COMSOL Multiphysics® software. This study examines the effect of trench depth at a fixed trench width on the sensitivity performance of the sensor. For further understanding, we discussed the electric field distribution throughout the sensor and effective RI changes at different analyte RI mediums as well as the corresponding physics involved.

2. Methodology

The investigated TCSF structure is illustrated in Figure 1. It consists of a TCSF with an outer diameter of 125 µm. Figure 1(a) depicts the 3-dimensional (3D) simulated structure of the TCSF sensor while Figure 1(b) shows the cross-section view of the TCSF with a sensing medium (analyte) in the cut-off region.

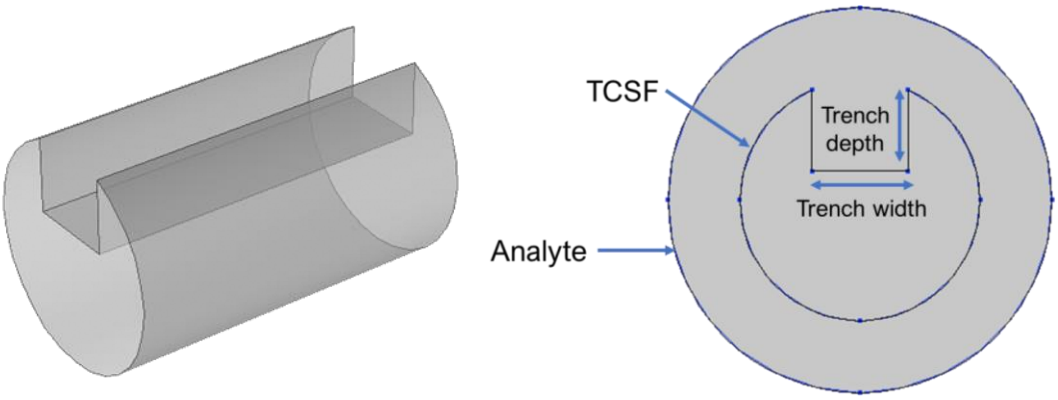

Fig. 1. The structure of TCSF in (a) 3D and (b) cross-section geometry

The simulation was executed by using the commercialized COMSOL Multiphysics 5.5® software (COMSOL). A two-dimensional (2D) space was chosen to simulate the sensing device instead of a 3D space to reduce the difficulty in the meshing process, large computer memory usage, and long simulation time. The wave optics module was selected to study the electrical field as the wavelength is comparable to or much smaller than the studied device. The cross-section method CSM was used to study the mode shape of the waveguide cross-section region by providing virtual information in the form of mode field diameter (MFD) [16,17]. While the sensor interacts with the analyte medium, the user can see the electric field distribution of the waveguide and analyze the penetration depth of the evanescent wave.

The geometry settings for CSM are shown in Table 1. The TCSF outer diameter domain wa set to 125 µm and the analyte domain diameter was set to 200 µm. The trench region was created at a fixed 50 µm width and various depths ranging from 0 µm, 10 µm, 30 µm, and 50 µm. Table 1 summarizes the geometry settings of the simulated model.

Table 1
Geometry settings

Domain	Dimension
Outer diameter	125 µm
Analyte diameter	200 µm
Trench width	50 µm
Trench depth	0 µm (TCSF0), 10 µm(TCSF10), 30 µm(TCSF30), 50 µm (TCSF50)

The material settings are used to assign the RI for each domain of the drawn geometry. A three-term Sellmeier equation is used to express the TCSF's RI at the near-infrared wavelength region as expressed in Eq. (1) [18]

$$n^2 - 1 = \frac{0.6961663\lambda^2}{\lambda^2-(0.0684043)^2} + \frac{0.4079426\lambda^2}{\lambda^2-(0.1162414)^2} + \frac{0.8974794\lambda^2}{\lambda^2-(9.896161)^2} \quad (1)$$

Here, n and λ is the TCSF RI and the operating wavelength, respectively. All the RI medium was set to isotropic medium. The TCSF and the analyte is made up of glass and liquid, respectively, thus possessing only one RI in all directions. The operating wavelength is set to 1550 nm, the minimum attenuation window in practical fiber. The parameters used are tabulated in Table 2.

Table 2
Material settings

Parameter	Value
TCSF RI	1.4440 RIU
Analyte RI	1.3000 RIU-1.4000 RIU
Medium RI	Isotropic

The sensing ability is owed to the interaction of the evanescent wave between the sensor and the analyte medium. The evanescent field 'senses' the changes in the RI distribution caused by the analyte medium, thus inducing the effective mode index, n_{eff} of the sensor. Penetration depth, d_p which represents the exponential decay of the evanescent wave with the distance in the analyte medium, can be expressed as in Eq. (2) [19]

$$d_p = \frac{\lambda}{2\pi\sqrt{n_{eff}^2 sin^2\theta - n_a^2}} \quad (2)$$

Here, λ and n_a is the operating wavelength and the analyte RI, respectively. From Eq. (2), the d_p value changes with the change in n_a. This allows for easy detection of unknown analyte RI medium. The sensor sensitivity, S can be expressed as in Eq. (3), which can be obtained from the slope of the graph

$$S = \frac{\Delta n_{eff}}{\Delta n_a} \quad (3)$$

3. Results and Discussion

Figure 2 shows the supported mode profile of the TCSF models. It is worth noting that, CSF allows multimode light propagation due to its large diameter size. However, the first six modes, including the fundamental mode are more significant to be studied as it carries most of the energy and are significantly excited for Gaussian beam excitation with relative power coupling efficiency >0.1% [17,20]. In this study, we only focus on the fundamental mode (LP_{01}) for the easiness in evaluation. In a selective study, the TCSF with different trench depths of 0 µm to 50 µm with respective electric field distributions are illustrated through red and blue color, representing the maximum and minimum electric field intensity, respectively. Generally, in the TCSF structure, the electric field is focused on the center and equally dispersed showing that the light is constrained in the fiber. Nevertheless, when increasing the trench depth, the electric field is shifted towards the bottom region boundary due to the lower RI contrast between the two mediums compared to that of trench region. The significant electric field shift was observed as the trench depth is increased to 50 µm. For all cases, the color faded out from red to blue indicating that the electric field gradually decreases when reaching the CSF/analyte due to the attenuation of the light energy as it reaches the boundary with different RI mediums.

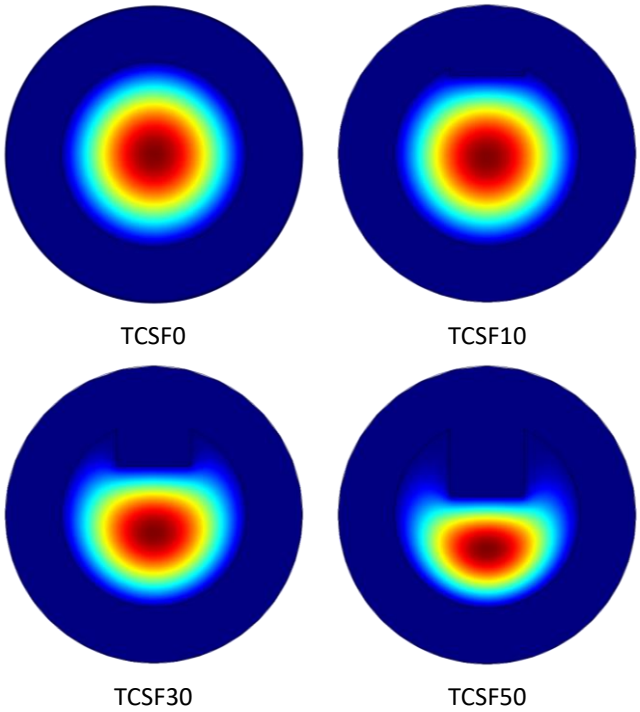

Fig. 2. Colored illustration of normalized electric field intensity around the TCSF

The electric field distribution of the TCSF can be analysed by studying the MFD at 1.3300 RIU as shown in Figure 3. A large variation of MFD can be seen when increasing the trench depth from 0 µm to 50 µm as shown in Figure 3(a). We separately plot the MFD for each TCSF as shown in Figure 3(b) to Figure 3(e) to show the penetration depth of the evanescent wave. From the graph, each design has a similar penetration depth, but the evanescent wave area increases as we increase the trench depth. For example, for TCSF0, the evanescent wave area is estimated to be 1.75×10^{-6} V^2 while for TCSF50, the estimated evanescent wave area is $4.00 \times 10^{-6} V^2$.

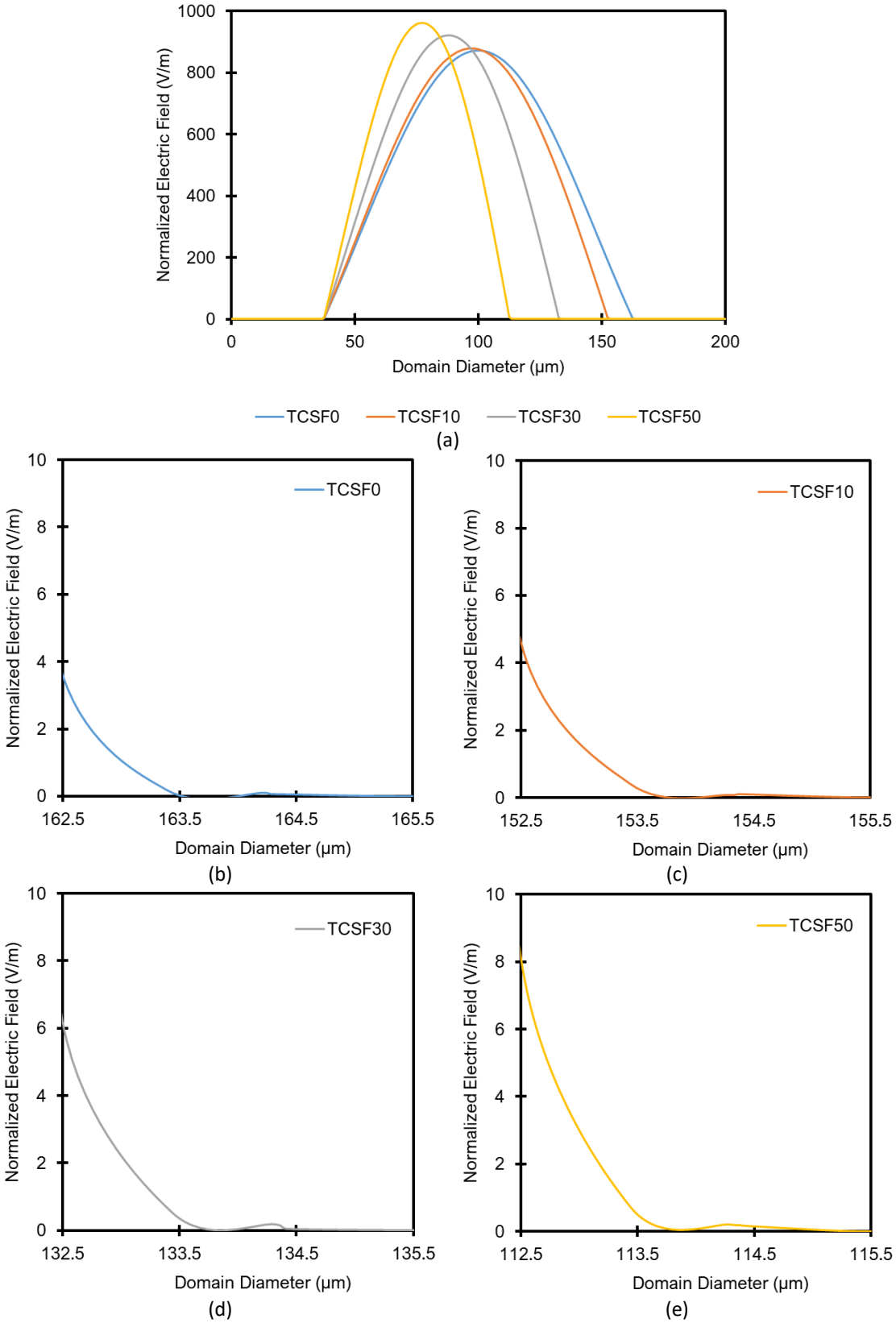

Fig. 3. MFD of the simulated design (a) in full plot and evanescent wave at the TCSF/analyte boundary for (b) TCSF0, (c) TCSF10, (d) TCSF30, (e) TCSF50

Figure 4 shows the MFD for TCSF0 and TCSF50 which represents the sensor towards the different analyte RI at the minimum and the maximum trench depth. The penetration depth depends on the RI difference between the TCSF and the analyte medium. By taking the TCSF0/cladding boundary as an example, the small RI difference between these two mediums causes a higher penetration depth to probe further into the cladding medium. However, this condition may lead to a less sensitive sensor due to the limited light interaction between the sensor and the analyte medium. In the case of TCSF50 which has 50 µm of trench depth, despite having the smallest penetration depth due to the high RI difference at the TCSF/analyte boundary, the full interaction between the evanescent wave and the analyte medium increases the sensor's sensitivity.

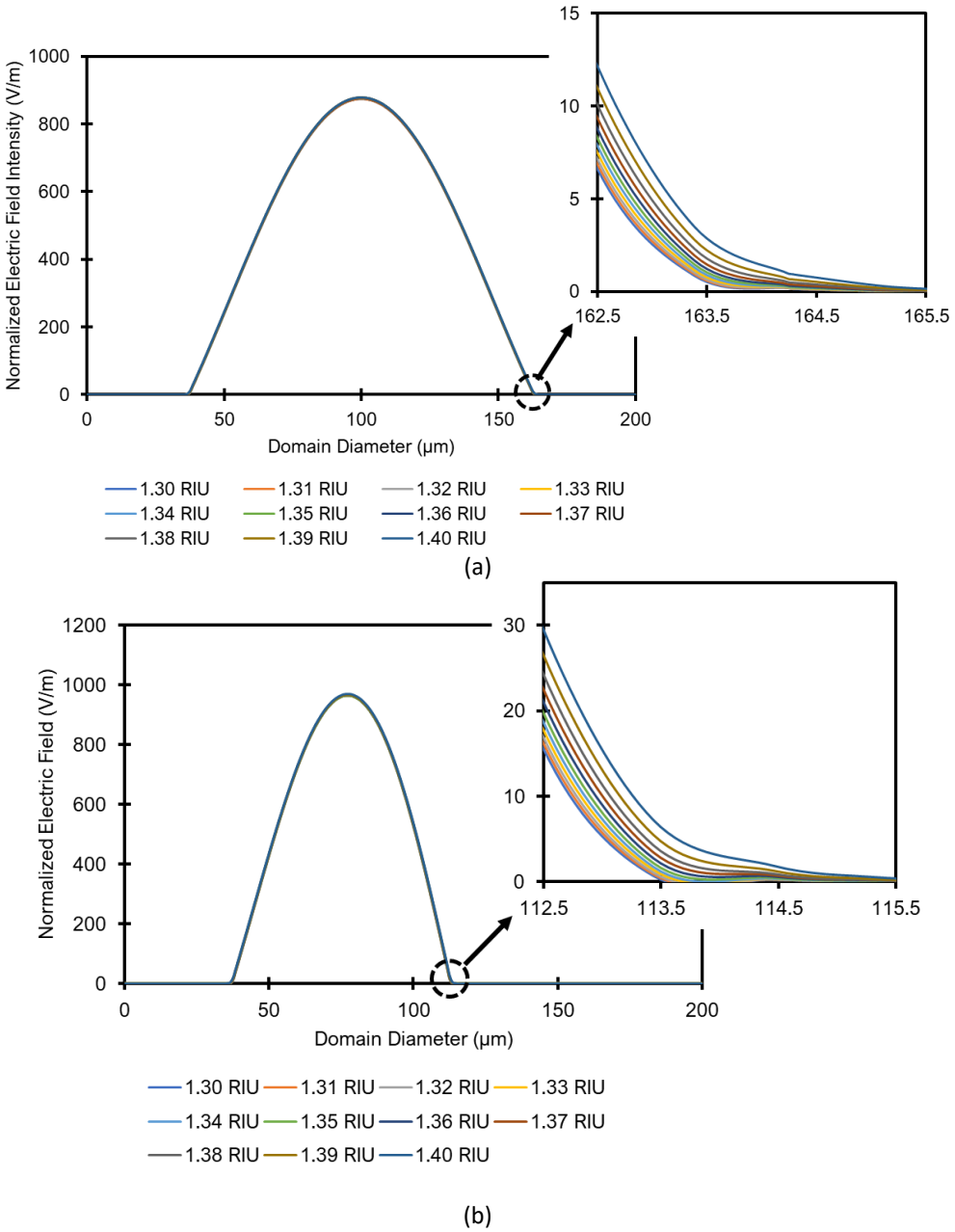

Fig. 4. The MFD at different analyte RI samples for (a) TCSF0 and (b) TCSF50. The inset shows the penetration depth of the evanescent wave. The initial value on the x-axis scale indicates the TCSF/analyte boundary

The n_{eff} changes at different analyte RI for each sensor design are plotted as shown in Figure 5. As shown in Figure 5(a), as the analyte RI increases from 1.3000 RIU to 1.4000 RIU, the n_{eff} changes also increase. An extremely small n_{eff} change occurred at TCSF0 and the n_{eff} changes are almost constant at a given analyte RI. However, the more significant n_{eff} changes were observed when increasing the trench depth to the maximum of 50 µm. Figure 5(b) shows the sensitivity changes towards the trench depth calculated at the highest analyte RI of 1.4000 RIU. The TCSF50 shows the highest estimated sensitivity of 6.62726x10^{-7}, and the TCSF0 shows the smallest sensitivity of 2.22053x10^{-7}, with total sensitivity changes of 4.40673x10^{-7}. This is expected since the evanescent wave highly 'senses' the disturbance from the analyte medium when the cladding layer is removed, causing more light interaction between the sensor and analyte medium. The simulation results agree with the simulation and experimental study of a side polished MMF, the closest design to the TCSF conducted by Chen *et al.,* [16] in which the sensitivity of the side polished MMF increases when increasing the polished region.

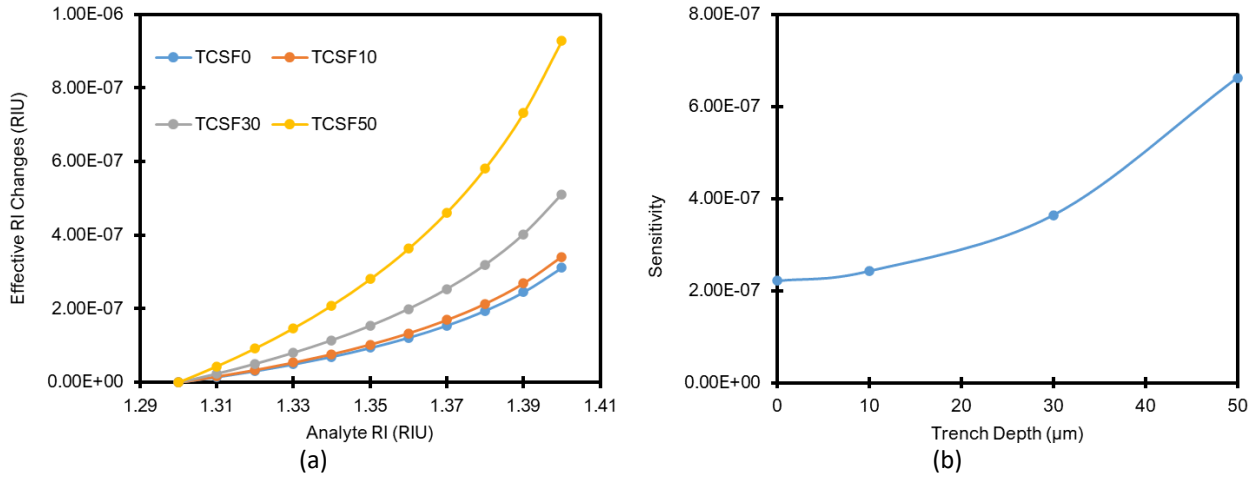

Fig. 5. (a) n_{eff} at different analyte RI and (b) the sensitivity for TCSF at different trench depths ranging from 0 µm to 50 µm

4. Conclusions

This work demonstrated the new unique design and simulation of TCSF sensor at different analyte RI ranging from 1.3000 RIU to 1.4000 RIU. The conducted design optimization at different trench depth is greatly helpful in determining the best TCSF sensor sensitivity. In the simulation evaluation, the optimized TCSF sensor measuring the different analyte RI shows different electric field distributions and evanescent fields without being overlapped. The highest estimated sensitivity achieved by the TCSF sensor is 6.62726x10^{-7} with 50 µm of trench depth. This sensitivity is higher than the simulated TCSF at 0 µm trench depth (or CSF) with an estimated sensitivity of 2.22053x10^{-7}. The simulated design evinced TCSF design as a convincing one for a new OFS type.

Acknowledgement
This research was not funded by any grant.

References

[1] Zhang, Ya-nan, Lebin Zhang, Bo Han, Peng Gao, Qilu Wu, and Aozhuo Zhang. "Reflective mercury ion and temperature sensor based on a functionalized no-core fiber combined with a fiber Bragg grating." *Sensors and Actuators B: Chemical* 272 (2018): 331-339. https://doi.org/10.1016/j.snb.2018.05.168

[2] Zhao, Yong, Jian Zhao, and Qiang Zhao. "Review of no-core optical fiber sensor and applications." *Sensors and Actuators A: Physical* 313 (2020): 112160. https://doi.org/10.1016/j.sna.2020.112160
[3] Wang, Qian, and Gerald Farrell. "All-fiber multimode-interference-based refractometer sensor: proposal and design." *Optics Letters* 31, no. 3 (2006): 317-319. https://doi.org/10.1364/OL.31.000317
[4] Chai, Quan, Hyeonwoo Lee, Seongjin Hong, Yongsoo Lee, Junbum Park, Jianzhong Zhang, and Kyunghwan Oh. "Nanoliter liquid refractive index sensing using a silica V-groove fiber interferometer." *Photonics Research* 7, no. 7 (2019): 792-797. https://doi.org/10.1364/PRJ.7.000792
[5] Wang, Fang, Kaibo Pang, Tao Ma, Xu Wang, Heng Lu, and Yufang Liu. "S-shaped refractometer based on dual tapered no-core fiber for low-range refractive index measurement." *Optics Communications* 463 (2020): 125419. https://doi.org/10.1016/j.optcom.2020.125419
[6] Kim, Taeyoon, Junha Jung, Jinho Lee, Geun Weon Lim, and Ju Han Lee. "Temperature-Insensitive Refractometer Based on a Wave-Shaped Fiber Modal Interferometer Using No-Core Fiber." *IEEE Sensors Journal* 21, no. 14 (2021): 16066-16077. https://doi.org/10.1109/JSEN.2021.3075473
[7] Zhao, Yeming, Zhengrong Tong, Weihua Zhang, Jietong Zhang, Jiaxin Li, and Xue Wang. "Refractive index Mach-Zehnder interferometer sensor based on tapered no-core fiber." *Laser Physics* 31, no. 4 (2021): 045101. https://doi.org/10.1088/1555-6611/abe241
[8] Sun, Bing, Fei Li, Kandi Xu, Kaiming Zhou, and Zuxing Zhang. "Temperature-insensitive fiber-optic refractometer based on immobilization of polydimethilsiloxane film." *IEEE Photonics Technology Letters* 34, no. 3 (2022): 165-168. https://doi.org/10.1109/LPT.2022.3144237
[9] Yang, Wenlei, Shuo Zhang, Tao Geng, Le Li, Guoan Li, Yijia Gong, Kai Zhang et al. "High sensitivity refractometer based on a tapered-single mode-no core-single mode fiber structure." *Sensors* 19, no. 7 (2019): 1722. https://doi.org/10.3390/s19071722
[10] Zhang, Mizhen, Guixian Zhu, Lidan Lu, Xiaoping Lou, and Lianqing Zhu. "Refractive index sensor based on ultrafine tapered single-mode nocladding single-mode fiber structure." *Optical Fiber Technology* 48 (2019): 297-302. https://doi.org/10.1016/j.yofte.2019.01.008
[11] Alsweefe, Huda, Sarah Kadhim Al-Hayali, and Abdulhadi Al-Janabi. "Efficient humidity sensor based on an etched no-core fiber coated with copper oxide nanoparticles." *Journal of Nanophotonics* 12, no. 4 (2018): 046018. https://doi.org/10.1117/1.JNP.12.046018
[12] Al-Hayali, Sarah Kadhim, and Abdul Hadi Al-Janabi. "All fiber-optic temperature sensor based on cladding etched no-core fiber coated with nanostructured copper oxide-polyvinyl alcohol thin film." *Optik* 220 (2020): 165154. https://doi.org/10.1016/j.ijleo.2020.165154
[13] Xiao, Gongli, Kaifu Zhang, Yuting Yang, Hongyan Yang, Ling Guo, Jianqing Li, and Libo Yuan. "Graphene oxide sensitized no-core fiber step-index distribution sucrose sensor." In *Photonics*, vol. 7, no. 4, p. 101. MDPI, 2020. https://doi.org/10.3390/photonics7040101
[14] Chauhan, Maya, and Vinod Kumar Singh. "ZnO nanostructures coated no-core fiber refractive index sensor." *Materials Science in Semiconductor Processing* 147 (2022): 106757. https://doi.org/10.1016/j.mssp.2022.106757
[15] Yi, Duo, Zhenwei Huo, Youfu Geng, Xuejin Li, and Xueming Hong. "PDMS-coated no-core fiber interferometer with enhanced sensitivity for temperature monitoring applications." *Optical Fiber Technology* 57 (2020): 102185. https://doi.org/10.1016/j.yofte.2020.102185
[16] Chen, Yaofei, Yuchan Hu, Hongda Cheng, Feng Yan, Qianyu Lin, Yu Chen, Pengjun Wu et al. "Side-polished single-mode-multimode-single-mode fiber structure for the vector magnetic field sensing." *Journal of Lightwave Technology* 38, no. 20 (2020): 5837-5843. https://doi.org/10.1109/JLT.2020.3003405
[17] Younus, Shahad I., Anwaar A. Al-Dergazly, and A. K. Abass. "Characterization of Multimode Interference Based Optical Fiber." In *IOP Conference Series: Materials Science and Engineering*, vol. 1076, no. 1, p. 012060. IOP Publishing, 2021. https://doi.org/10.1088/1757-899X/1076/1/012060
[18] Malitson, Ian H. "Interspecimen comparison of the refractive index of fused silica." *Journal of the Optical Society of America* 55, no. 10 (1965): 1205-1209. https://doi.org/10.1364/JOSA.55.001205
[19] Agnarsson, Björn, Saevar Ingthorsson, Thorarinn Gudjonsson, and Kristjan Leosson. "Evanescent-wave fluorescence microscopy using symmetric planar waveguides." *Optics Express* 17, no. 7 (2009): 5075-5082. https://doi.org/10.1364/OE.17.005075
[20] Datta, Arijit, Appasani Mahendra Babu, and Ardhendu Saha. "Enhanced sensitivity of fiber optic evanescent wave absorption-based concentration sensor by shining a Bessel-Gauss beam and effect of fiber bending on the sensor response: a theoretical analysis." *Optical Engineering* 58, no. 5 (2019): 056112. https://doi.org/10.1117/1.OE.58.5.056112